ANALYSIS OF TRANSONIC NOZZLE LOSS GENERATION IN ORGANIC RANKINE CYCLE (ORC) TURBINES

Tao Chen[1], Peter J. Newton[1], Miles C. Robertson[1], Ricardo F. Martinez-Botas[1] *

[1]Department of Mechanical Engineering, Imperial College London,
London, SW7 2AZ, United Kingdom
Email: r.botas@imperial.ac.uk

*Corresponding author, email: r.botas@imperial.ac.uk

ABSTRACT

The Organic Rankine Cycle (ORC) is a technology facilitating the generation of useful mechanical power, from a wide variety of low-temperature heat sources. The specific application considered in this paper is heavy-duty vehicles, as part of a secondary (or bottoming) cycle. A single stage high-expansion-ratio turbine is a suitable type of expander for this application, the nozzle would be transonic given the high expansion ratios. This paper analyses the loss generation mechanisms within the transonic nozzle, with a view towards improving the design of high-pressure ratio turbine expanders for an increasing stage efficiency.

This paper simulates the transonic flow of R1233zd(E) in a linear nozzle blade cascade by means of Computational Fluid Dynamics (CFD). The cascade is designed to achieve a uniform outlet flow Mach number of 2. An initial analysis uses irreversible entropy generation rate to study and explain the loss generating mechanisms in the nozzle under on- and off-design conditions, and the entropy loss coefficient is used to quantitatively analyse the loss distribution. The loss generated in the expansion process takes 28.2 % of the overall loss, and the loss in the region after expansion takes the remaining 71.8 %.

The impact of real-gas properties is then considered by comparing with an equivalent air cascade. The loss generated in the expansion process for the R1233zd(E) cascade is 19.7 % larger than that for air due to a larger non-ideal expansion loss. The loss generated in the region after the expansion process for the R1233zd(E) cascade is 11.4 % lower than that for air due to a lower loss caused by trailing-edge wave and trailing-edge wake. The overall loss is 4.4 % lower in the R1233zd(E) cascade; conversely, the total pressure loss coefficient is 13.8 % larger in the R1233zd(E) cascade than that in the air cascade. This is explained by an analysis of Gibbs entropy formula for a real-gas which shows that the stagnation pressure loss is attributed to both an entropy gain and a real gas effect.

1. INTRODUCTION

The idea of using a small-scale ORC system to recover waste heat in heavy-duty mobile applications has gained interest in the last decade. Before these systems can become commercially viable it will be necessary to maximize their performance. One of the key components that drives both the cost and overall efficiency of the system is the expander, therefore this paper concentrates on this component.

One of the primary candidate expander types for small-scale (10-20 kW) ORC systems is the use of a turbine. These hold several advantages for mobile heavy duty applications, including their high volumetric power density and relative simplicity. These turbines typically operate under a high expansion-ratio and often require a transonic nozzle to enable effective power conversion (Costall *et al*., 2015). Wheeler and Ong (2013, 2014) developed a design method for a high-pressure-ratio turbine nozzle ring. Their work highlighted in the importance of the interaction between nozzle trailing-edge shocks and rotor leading-edge in governing the aerodynamic losses in the stage. Meanwhile, Pini *et al*.

(2017) showed that the loss generated in the nozzle can account for nearly 50 % of the total loss in an ORC turbine. These investigations underline the importance of correctly understanding the flow structure and loss generation mechanisms in a transonic nozzle to improve ORC turbine efficiency.

In light of this, this work studies the flow in a transonic linear cascade by computational fluid dynamics (CFD) simulation. The use of a linear cascade was chosen as a simple geometric configuration to understand basic flow in turbomachinery and also with a view to future experimental work that will be used to validate these simulations. Refrigerant R1233zd(E), trans-1-chloro-3,3,3-trifluoropropene (chemical formula:$CF_3CH{=}CHCl$), is used as the working fluid for this research, with the main properties of this fluid shown in Table 1. This fluid has a low 100-year global warming potential and has been shown to be a contestant fluid for large internal combustion engine applications (Eyerer *et al.*, 2016).

Table 1: Main properties of R1233zd(E)

Properties	**Value**	**Properties**	**Value**
Critical temperature (K)	438.75	GWP_{100}	7
Critical pressure (kPa)	3772.1	ODP	0.00034
Molecular mass (kg/kmol)	134.03	ALT (days)	26
Condensing pressure at 40°C (kPa)	214.5	Flammability	Non flammable
Slope ds/dT	Positive	Toxicity	Non toxic

*data in this table comes from: Søndergaard *et al.*(2007), Patten and Wuebbles (2010), Hulse *et al.*(2012).

The paper firstly discusses the flow structure and loss generation distribution of the linear cascade based on the simulation results for both on- and off-design conditions using R1233zd(E). The analysis then goes on to compare the flow in the R1233zd(E) cascade with that of an equivalent cascade using air as a working fluid. The similarities and differences between the performance of the nozzles with the two different fluids are discussed.

2. DESIGN METHOD OF THE LINEAR CASCADE

A sketch of a typical linear cascade for illustration only is shown in Fig. 1(a), where θ_{in} and θ_{out} represent the inlet and outlet flow angles respectively, and α_l and α_t are the leading-edge and trailing-edge blade angles. The blade pitch S_c is defined as the distance between the edges of two adjacent blades. The actual blade profile for the transonic nozzle used in this work can be seen in Fig. 1(b). This can be separated into three regions: the convergent (sub-sonic, red curve) section, the divergent (super-sonic, blue curve) section and the trailing-edge section (yellow line). The cascade is two dimensional and so the full three-dimensional geometry is represented by a straight extrusion of this profile to the blade height (5mm). In this figure l_{th} is the throat width, l_{end} is the nozzle width at the end of the divergent section, l_b is the blade length and T_t is the thickness of blade trailing-edge.

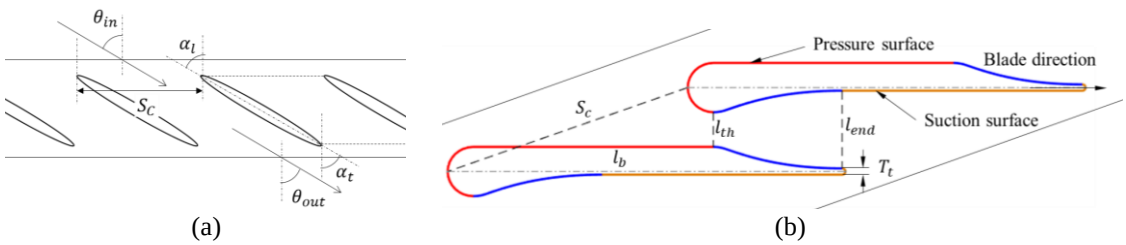

(a) (b)

Figure 1: Geometry of a transonic linear cascade (a), and the cascade geometry studied in this paper (b)

The design of the cascade nozzle is carried out in two steps. Firstly, the divergent section is designed by the method of characteristics (MOC) for a real gas (Wheeler and Ong, 2013), to achieve a 'shock-free' expansion to a design Mach number. The design of the convergent and trailing-edge sections of the blade are then determined, based around the super-sonic nozzle profile, the trailing edge thickness, blade length and blade angles. The profile of the leading-edge and trailing-edge sections of this cascade consist of a semi-circle adjoining to a straight tangent line. The main parameters of the linear cascade

studied in this work are listed in Table 2. Theoretical outlet Mach number and pressure are the values at the end of divergent section, which does not consider the influence of the blade trailing edge.

Table 2: Design parameters of the transonic linear cascade

Parameters	**Value**	**Parameters**	**Value**
Leading-edge blade angle α_l (°)	70	Throat width l_{th} (mm)	5.56
Trailing-edge blade angle α_t (°)	70	Width at the end of divergent section l_{end} (mm)	12.42
Blade pitch S_c (mm)	39.23	Trailing-edge thickness T_t (mm)	1
Blade length l_b (mm)	60.07	Blade height H (mm)	5
Inlet total pressure (kPa)	1700	Theoretical Mach number (-)	2
Inlet total temperature (K)	400	Theoretical outlet static pressure (kPa)	210.53
Mass flow rate per passage (kg/s)	0.2	Theoretical pressure ratio (-)	8.07

3. SIMULATION AND ANALYSIS METHOD

All calculations in this work were performed in ANSYS CFX using the steady Reynolds-averaged Navier–Stokes (RANS) equations with a k-ε turbulence model. A hexahedral mesh was generated in ANSYS ICEM, the grid convergence is shown in Fig. 2, and the final element number per passage was 4,464,852 for the R1233zd(E) nozzle and 4,379,536 for the air nozzle. This included two chord lengths upstream of the nozzle and 7 chord lengths downstream. A mesh independence study showed that grid convergence was achieved at around 3 million elements in each case (y^+ ~30-100) with respect to the main flow structures of interest, in particular the resolution of the trailing edge wave system. A Peng-Robinson equation of state (PR-EoS) is used for all simulations containing R1233zd(E), and the zero-pressure specific heat capacity is fitted by a fourth order polynomial. Parameters in the PR-EoS are determined by experimental data (Hulse *et al.*, 2012). The dynamic viscosity and the thermal conductivity of R1233zd(E) are simulated by kinetic theory model in ANSYS CFX. When computing the air a perfect gas is assumed with $\gamma = 1.4$.

The configuration of the numerical simulations in this study are based upon those of Robertson *et al.* (2019), who obtained static pressure measurements along the centre line of a Mach 2 transonic nozzle using R1233zd(E). Their study showed that the numerical results captured the trend of the experimental data well. Even so, the maximum averaged difference between the measured value and the simulated static pressure is 16.4 % for R1233zd(E) using PR-EoS, this was superior to the results obtained when an ideal gas assumption was made, which showed a case average deviation of 19.6 %. These deviations do not account for the experimental uncertainty, nevertheless, this difference shows the importance of the choice of the equation of state.

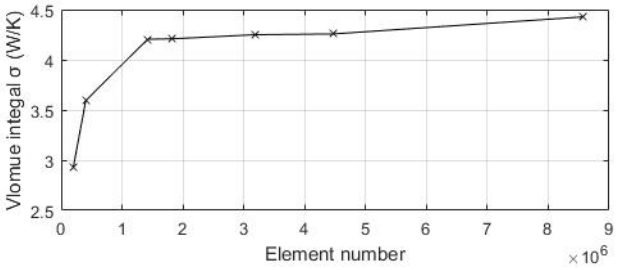

Figure 2: Grid convergence by volume integral the entropy generation rate (σ) over the flow domain.

An important aspect of this work is the understanding of the loss mechanisms within the cascade. Here the entropy generation rate (σ) was used in a qualitative manner to present the loss generation. This is defined in Eq. (1) (Woods,1975) and represents irreversible entropy production rate per unit volume. Consideration of momentum and energy conservation lead to Eq. (2) when no external radiative source of heat is considered. To apply this equation to RANS simulation results, Eq. (3) is derived from Eq.

(2) under the Reynolds Averaging method and turbulent-viscosity hypothesis, where the real-gas EoS must be used, Eq. (4).

$$\dot{m}\frac{ds_{irrev}}{dt} = \iiint_{V_{system}} \sigma dV \tag{1}$$

$$T\sigma = -\frac{\dot{\boldsymbol{q}}}{T}\cdot\nabla T + \tau_{ij}\frac{\partial u_i}{\partial x_j} \tag{2}$$

$$T\sigma = \frac{\left(k+\Gamma_T c_p\right)}{T}\left(\frac{\partial T}{\partial x_i}\right)^2 + \frac{\Gamma_T}{T}\left(\frac{\partial h}{\partial p}\right)_T\left(\frac{\partial p}{\partial x_i}\right)\left(\frac{\partial T}{\partial x_i}\right) + (\mu+\mu_T)\left[\left(\frac{\partial \bar{U}_\iota}{\partial x_j}+\frac{\partial \bar{U}_J}{\partial x_i}\right) - \frac{2}{3}\frac{\partial \overline{U_k}}{\partial x_k}\delta_{ij}\right]\frac{\partial \bar{U}_\iota}{\partial x_j} \tag{3}$$

$$dh = c_p dT + \left(\frac{\partial h}{\partial p}\right)_T dp \tag{4}$$

An entropy loss coefficient ε^s is also defined in Eq. (5), which was used for analysing the losses within a cascade quantitatively by dividing the nozzle into streamwise sub-regions. It is defined by the increase of entropy from the inlet boundary of the nozzle to the outlet of each sub-region, normalized by the specific gas constant $R = \boldsymbol{R}/M$, where $\boldsymbol{R}$ is the universal gas constant ($\boldsymbol{R} = 8.314\ J/(mol\cdot K)$) and M represents the molecular mass of the fluid. Another useful metric in studying the losses within a cascade is the total pressure loss coefficient, this can be used to highlight some of the effects of real-gas behavior, which are not apparent when using the entropy loss coefficient ε^s alone. The total pressure loss is defined by the drop of mass-flow-averaged total pressure from the nozzle inlet boundary to the outlet of each sub-region normalized by the total pressure at the inlet boundary, Eq. (6).

$$\varepsilon^s = \frac{\overline{s_{out}}^M - \overline{s_\infty}^M}{R} \tag{5}$$

$$\varepsilon^p = \frac{\overline{p_{0,\infty}}^M - \overline{p_{0,out}}^M}{p_{0,\infty}} \tag{6}$$

4. RESULTS

4.1 Flow Structure in the Linear Cascade with R1233zd(E) – On- and Off-Design

The flow field of the linear cascade was simulated under three working conditions, see Table 3. Case 2 refers to the design condition, while Case 1 refers to an over-expanded condition (back pressure decreased by 50 %) and Case 3 refers to an under-expanded condition (back pressure increased by 50 %). Mach number distribution on the mid-span plane of the cascade is shown in Fig. 3. The flow field can be divided into two main regions: an expansion region (upstream of the dashed line in Fig. 3) and a trailing-edge region (downstream of the dashed line in Fig. 3). In the expansion region the fluid accelerates to the designed Mach number. In this cascade, the mass flow average Mach number at the outlet of the expansion region is 1.92 in Case 2, which is 4 % lower than the expected design value. In the trailing-edge region, the fluid leaves the cascade through an upward trailing-edge wave system (I), a reflected wave system (II) and a downward trailing-edge wave system (III). Each of these three trailing-edge wave systems consists of three parts: an expansion fan followed by a compression shock wave in the middle and then another weak expansion fan behind the shockwave. A trailing-edge wake (IV), which is a free shear wake, downstream the blade trailing edge will also influence the flow in the trailing-edge region.

Table 3: Inlet and outlet conditions of the simulation

Parameters	Case 1 (over-expanded)	Case 2 (design point)	Case 3 (under-expanded)
Inlet total pressure (kPa)	1,700	1,700	1,700
Inlet total temperature (K)	400	400	400
Outlet static pressure (kPa)	105.27	210.53	315.80795

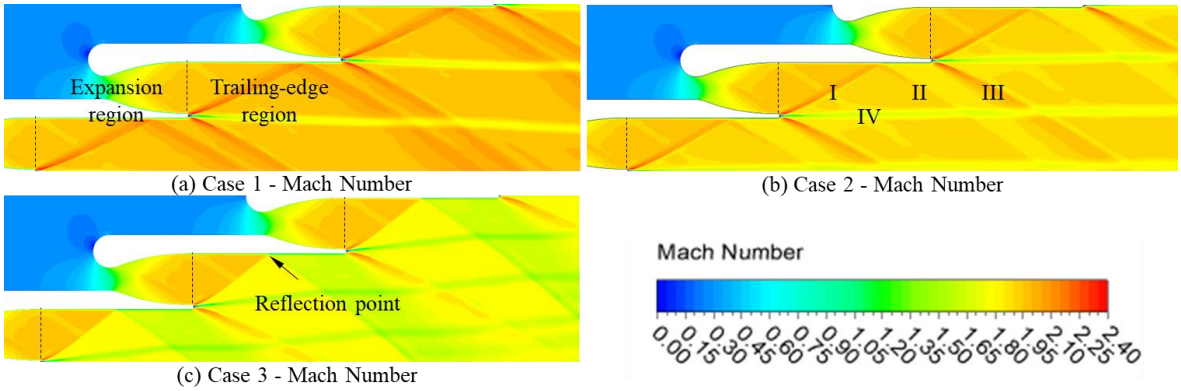

Figure 3: Mach number distribution on the mid-span plane of the cascade

The flow in the expansion region is not influenced by the outlet pressure, however, this is not the case in the trailing-edge region. As shown in Fig. 3, when the outlet pressure increases, the propagating angle of the trailing-edge wake, which is determined by the fluid flow angle, (see Feature IV in Fig. 3(b)) will increase (-2.2°, 1.0°, 5.7° for Case 1, Case 2, Case 3 respectively). The propagating angle of the upward trailing-edge wave (see Feature I in Fig. 3(b)) also increases when the outlet pressure increases (28.2°, 30.3°, 38.2° for Case 1, Case 2, Case 3 respectively), consequently the reflection point on the blade surface also moves forward by 17 % of the blade chord in from Case 1 to Case 3.

4.2 Distribution of Loss Generation

The entropy generation rate (σ) distribution on the mid-span plane and the 15 % span plane in all three cases are shown in Fig. 4. In general, it was found that the losses could be divided into five main sources for all cases. The first three are all due to viscid effects: the boundary layer loss due to the friction on the blade profile and endwalls, the trailing wake loss (see Fig. 4(a)), which emanates from the blade profile boundary layer, and the leading edge loss (see Fig. 4(d)), which results from the interaction between the endwall boundary layer and the leading edge of the blade. The other two losses are wave losses: shock loss (see Fig. 4(d)) due to the large velocity gradient in trailing edge shock waves, and the non-ideal expansion loss, which due to the unexpected weak shock waves in supersonic region of the expansion process. The non-ideal expansion loss can be seen clearly in Fig. 5, which shows a contour plot of entropy on the blade mid-span plane.

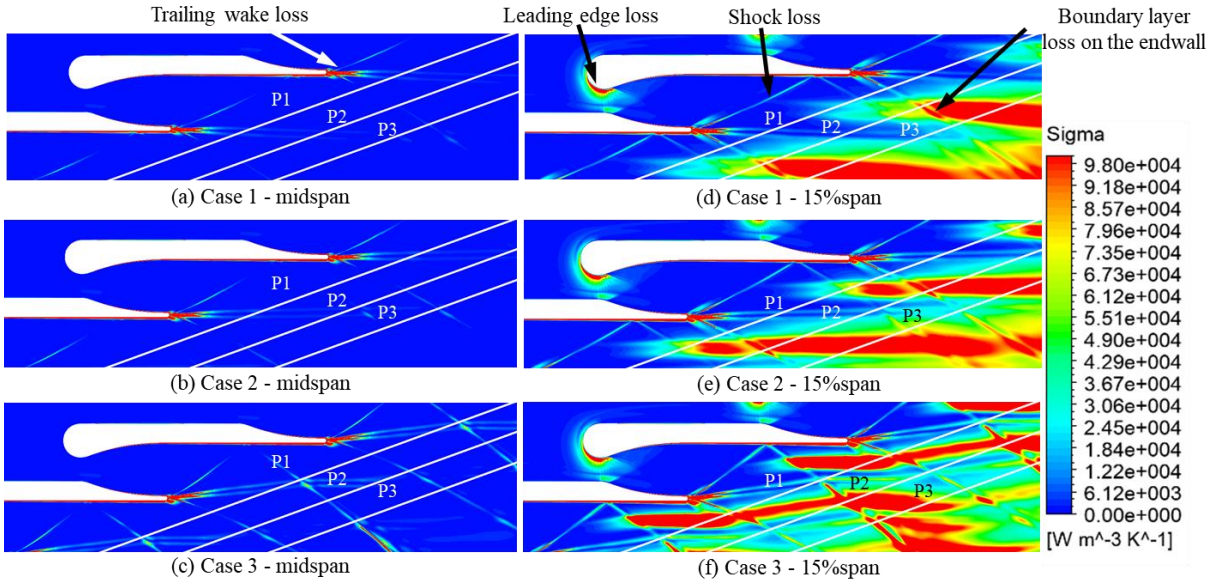

Figure 4: Entropy generation rate (σ) distribution in different cases and different span planes

The loss generation distribution in the expansion region is very similar in each case, while, as expected, the trailing-edge region loss is influenced by the back pressure. As the back pressure increases, the interaction between shock waves and endwall boundary layers lead to an increase in the boundary layer thickness, so the endwall boundary layer region, which can be seen on the 15 % span plane, moves forward from plane P2 in Case 1 (see Fig. 4(d)) to plane P1 in Case 2 (see Fig. 4(e)) and further front in Case 3. Plane P1, P2 and P3 represent the planes at 0.5, 1, $1.5S_c$ downstream the blade trailing edge.

To compare the loss distribution quantitatively, the cascade is separated into streamwise sub-regions, which are shown in Fig. 6(a). The entropy loss coefficient ε^s was then evaluated in each of these sub-regions and shown in Fig. 6(b). It shows that the loss generation in these three cases is almost identical from leading edge to the end of expansion region. The value of ε^s is 0.071 at the end of the expansion region. After that ε^s diverges between the different cases. The entropy loss coefficient for Case 2 (design condition) at $1.5S_c$ downstream of the trailing edge is 0.252, which is slightly higher than those in Case 1 and in Case 3 by 4.1 % and 2.0 % respectively. These figures show that in the design case the loss generated during the expansion process takes 28.2 % of the overall value, while the loss generated in the trailing-edge region accounts for the remaining 71.8 %. This is congruent with the findings of Wheeler and Ong (2013, 2014) who emphasize the significance of the trailing edge wave system in ORC turbine design.

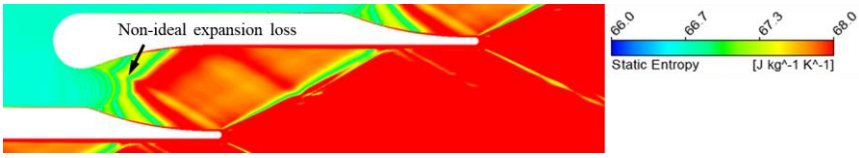

Figure 5: Entropy distribution in mid-span plane in Case 2

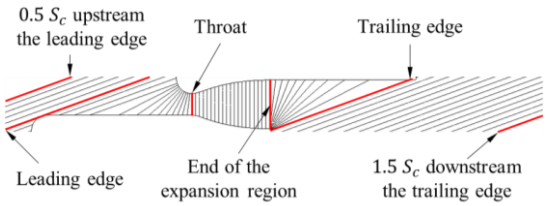

(a) Position of the sub-regions

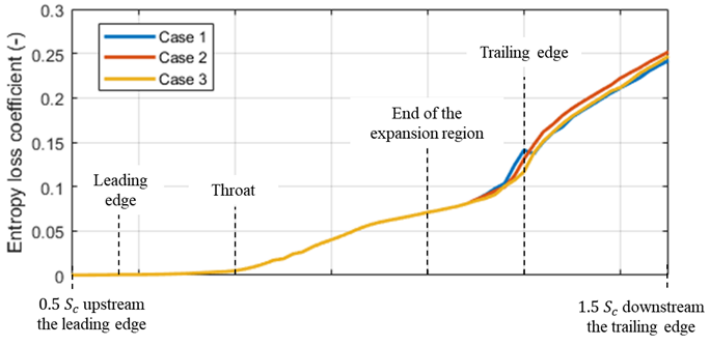

(b) Entropy loss coefficient

Figure 6: Entropy loss coefficient distribution in different cases

4.3 Comparison with an air cascade

The R1233zd(E) cascade is compared with an equivalent air cascade at the design condition to analyze the impact of real gas properties. The air cascade is designed by the same method described in Section 2. The throat area, trailing-edge thickness and the Mach number at the outlet of the divergent section are kept the same as that of the R1233zd(E) cascade. The flow field in the air cascade is simulated by the method introduced in Section 3, and the inlet condition is the same as that of the R1233zd(E) cascade, whilst the outlet pressure is set to 217 kPa.

The Mach number distribution of the air cascade is shown in Fig. 7(a). The mass flow average Mach number at the outlet of the expansion region is 1.96, which is 2 % lower than expected, this is closer to the target design value than for the R1233zd(E) cascade, which gave a Mach number of 1.92. Compared with Case 2 for the R1233zd(E) cascade (design case, see Fig. 3(b)), the decrease in Mach number across the upward trailing-edge wave and the reflected wave is more significant in the air cascade. The distribution of entropy generation rate σ is shown in Fig. 7(b) & (c), which can be compared directly with that for the R1233zd(E) cascade in Fig. 4(b) & (d). This qualitative comparison shows that the system of losses in each case is largely similar in the two cases.

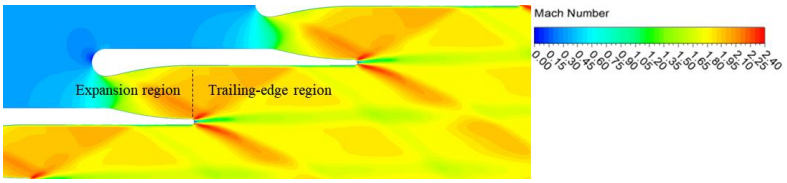

(a) Mach number distribution

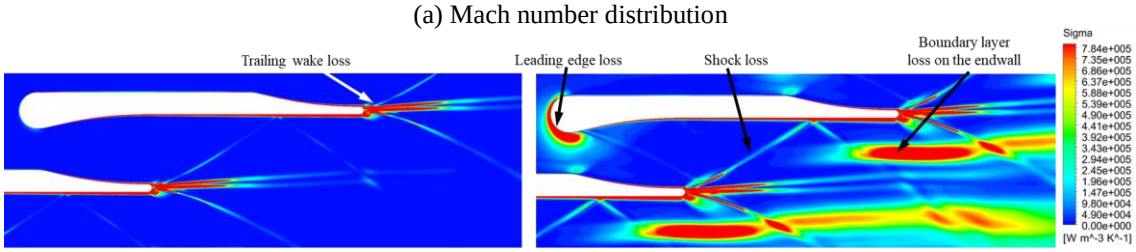

(b) σ distribution on mid-span (c) σ distribution on 15% span

Figure 7: Flow field of the air cascade

A comparison of streamwise entropy loss coefficient in the two fluids is shown in Fig. 8(a). Up to the throat the entropy loss coefficient for the R1233zd(E) falls below that for air, but subsequently starts to increase faster than that for air until around halfway through the diverging section of the nozzle. By the end of the expansion region, the entropy loss for the R1233ze(E) cascade is 19.7 % larger than that for the air. This larger loss is caused by the significant non-ideal expansion loss in the diverging section of the nozzle, which can be seen in Fig. 5. A similar loss was not evident in the air cascade. After the expansion process, the loss in the air cascade increases faster than that for the R1233zd(E) and by $1.5S_c$ downstream of the trailing edge the entropy loss coefficient in the R1233zd(E) cascade is 4.4 % lower than that for air. The increase in entropy loss coefficient from the end of the expansion region to $1.5S_c$ downstream of the trailing edge is 11.4 % greater in air than for R1233zd(E). This area of loss is heavily influenced by the trailing edge wave system and the wake from the blade. Even though both of these loss systems are qualitatively similar between air and R1233zd(E), their effect is clearly different.

In order to enable a comparison to entropy loss in Fig. 8(a), the streamwise mass flow average total pressure loss coefficient ε^p is shown in Fig. 8(b). This shows that the R1233zd(E) cascade ε^p is 13.8 % higher than that for air by $1.5S_c$ downstream of the trailing edge. This is surprising given that ε^s was 4.4 % lower for R1233zd(E) than for air. The seemingly inconsistent results from these two loss coefficients, which are equivalent for perfect gases, is caused by real-gas effects. For a fluid, Gibbs entropy formula, Eq. (7), can be derived into Eq. (8) when considering a real gas equation of state, shown by Eq. (9) and the enthalpy equation Eq. (4). It should be mentioned that the specific heat capacity at constant pressure c_p and the compressibility factor Z are both binary functions of temperature and pressure. By integrating Eq. (8) from reference state to a specific state, Eq. (10) results. Equation (10) can also be used in a stagnation state, so the entropy gain is equal to $-R\ln(p_0/p_{0,ref})$ for a perfect gas in an adiabatic process. However, for a real gas, the first and the third terms in Eq. (10) cannot be neglected. In Fig. 9, $(s-s_{ref})/R$ and $-\ln(p_0/p_{0,ref})$ along nozzle centre line are compared. This figure shows that $(s-s_{ref})/R$ is lower than $-\ln(p_0/p_{0,ref})$, for the ORC nozzle. The average relative difference between these two terms is 33 % in the region from the throat to 1.5 S_c downstream the trailing edge. This difference can be directly attributed to the real gas behavior on the

stagnation pressure loss. The stagnation pressure loss can be divided into two components, one due an increase in entropy, and secondly a real gas component. In the absence of heat flux, the entropy component of the stagnation pressure loss is irreversible, as opposed to the real gas component, which is a reversible process. This shows the value of including real gas effects in such simulations and that care must be exercised in relating between stagnation pressure loss and entropy gain.

$$Tds = dh - vdp \tag{7}$$

$$ds = c_p \frac{dT}{T} + \left(\frac{\partial h}{\partial p}\right)_T \frac{dp}{T} - ZR\frac{dp}{p} \tag{8}$$

$$pv = ZRT \tag{9}$$

$$s - s_{ref} = c_{p,ref}\ln\left(\frac{T}{T_{ref}}\right) - R\ln\left(\frac{p}{p_{ref}}\right) + \int \left(c_p - c_{p,ref}\right)\frac{dT}{T} + \left(\frac{\partial h}{\partial p}\right)_T \frac{dp}{T} + (1-Z)R\frac{dp}{p} \tag{10}$$

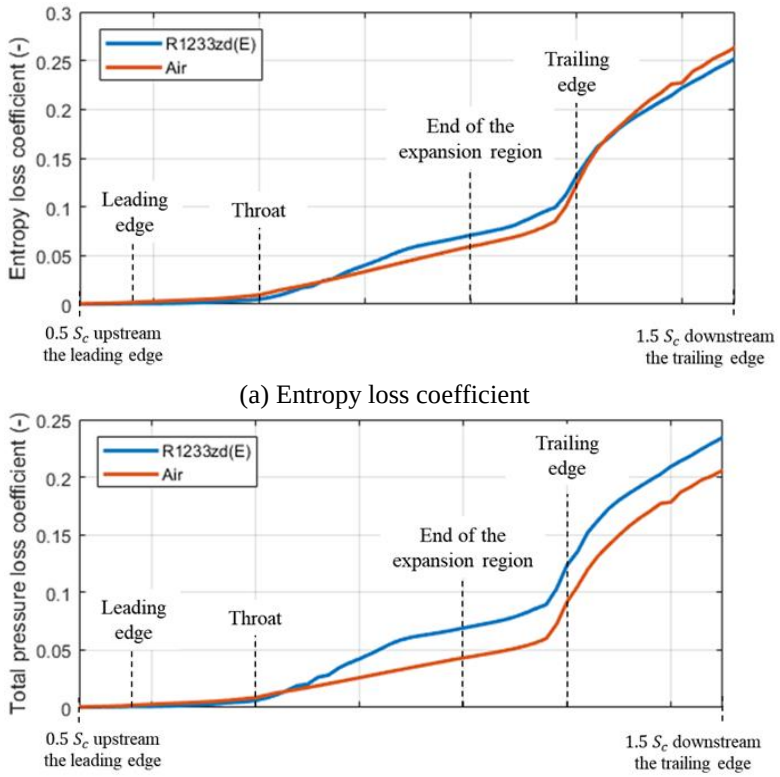

(a) Entropy loss coefficient

(b) Total pressure loss coefficient

Figure 8: Comparison of the entropy loss coefficient and the total pressure loss coefficient between the air cascade and the R1233zd(E) cascade

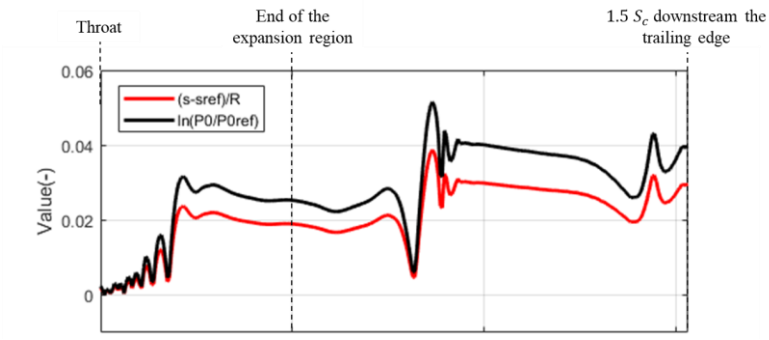

Figure 9: Comparison of $(s - s_{ref})/R$ and $-\ln(p_0/p_{0,ref})$ along the nozzle centre line

5. CONCLUSIONS

A cascade for R1233zd(E) is designed and simulated under three different operating conditions in this work. It is found that back pressure does not influence the flow in the nozzle expansion region, whilst having a significant influence downstream of the trailing edge. As the back pressure increases by 50 %, the flow angle in the region after the trailing-edge wave will increase from 1.0° to 5.7°, while as the back pressure decreases by 50 %, it decreases to -2.2°. The loss distribution in the cascade is analysed and five main sources of the loss generation are identified. Three of them are caused by viscid effects and two of them are wave losses. In the design condition, the loss generated during the expansion process makes up 28.2 % of the overall entropy loss coefficient with the remaining 71.8 % in the trailing edge region, which is largely influenced by the shockwave system and trailing edge wake. This result highlights the importance of these features during turbine design. The back pressure has limited influence on the loss generation in the cascade, and the maximum overall entropy loss coefficient difference between on- and off-design conditions is 4.1 %.

Secondly, this cascade is compared with an equivalent air cascade. It shows that the R1233zd(E) cascade has a larger non-ideal expansion loss in the divergent region of the nozzle, so it has a 19.7 % larger entropy loss coefficient in the expansion process than that for the air cascade. Downstream of the diverging section of the nozzle, where the shockwave system and trailing edge wake are dominant flow features, the increase in the entropy loss coefficient for R1233zd(E) is 11.4 % lower than that for the air cascade. The overall entropy loss coefficient in the R1233zd(E) cascade is 0.252 which is 4.4 % lower than that in the air cascade. Conversely, the total pressure loss is 13.8 % larger in the R1233zd(E) cascade than that in the air cascade. By an analysis of Gibbs entropy formula, it was shown that the stagnation pressure loss consists of an entropy gain component and also a component due to real gas effects. A comparison of the entropy gain against the logarithm of the stagnation pressure ratio showed that entropy change was 33 % lower for the refrigerant than expected for an ideal gas, where both of these terms are equivalent in the absence of heat transfer. Therefore, the entropy loss coefficient should not be thought of equivalent to the total pressure loss coefficient in a real gas and caution should be taken in interchanging these values.

ACKNOWLEDGEMENTS

The research was funded in part by the China Scholarship Council (CSC).

NOMENCLATURE

c_p	specific heat capacity at constant pressure	(J/(kg·K))
h	enthalpy	(J/kg)
k	thermal conductivity	(W/(m·K))
p	pressure	(kPa)
$\dot{\boldsymbol{q}}$	heat transfer rate	(W/ m^2)
s	entropy	(J/(kg·K))
T	temperature	(K)
t	time	(s)
$\bar{U}$	Reynolds-averaged velocity	(m/s)
u	velocity	(m/s)
V	volume	(m^3)
y^+	Y plus	(-)
Γ_T	turbulent diffusivity	(kg/(m·s))
δ_{ij}	Kronecker delta	(-)
μ	dynamic viscosity	(Pa·s)
σ	entropy generation rate	(W/(m^3·K))
$\tau_{i,j}$	viscous stress	(kg/(m·s^2))

Superscript

+	plus
p	pressure
s	entropy
M	mass flow rate averaged

Subscript

0	total value
∞	value at $0.5S_c$upstream of leading edge
irrev	irreversible

REFERENCES

Costall, A. W., Hernandez, A. G., Newton, P. J., & Martinez-Botas, R. F., 2015, Design Methodology for Radial Turbo Expanders in Mobile Organic Rankine Cycle Applications. *Appl. Energy*, vol. 157, p. 729-743.

Eyerer, S., Wieland, C., Vandersickel, A., & Spliethoff, H., 2016, Experimental Study of an ORC (Organic Rankine Cycle) and Analysis of R1233zd-E as a Drop-in Replacement for R245fa for Low Temperature Heat Utilization, *Energy*, vol. 103, p. 660-671.

Robertson, M. C. Newton P. J., Chen T., Martinez-Botas R. F., 2019, Development and Commissioning of a Blowdown Facility for Dense Gas Vapours, *Proceedings of ASME Turbo Expo 2019: Turbine Technical Conference and Exposition* (in press)

Hulse, R. J., Basu, R. S., Singh, R. R., & Thomas, R. H., 2012, Physical Properties of HCFO-1233zd (E), *J. Chem. Eng. Data*, vol. 57, no. 12: p. 3581-3586.

Patten, K. O., & Wuebbles, D. J. (2010). Atmospheric Lifetimes and Ozone Depletion Potentials of Trans-1-chloro-3, 3, 3-trifluoropropylene and Trans-1, 2-dichloroethylene in a Three-dimensional model, *Atmos. Chem. Phys.,* vol. 10, no. 22: p. 10867-10874.

Pini, M., De Servi, C., Burigana, M., Bahamonde, S., Rubino, A., Vitale, S., & Colonna, P., 2017, Fluid-dynamic Design and Characterization of a Mini-ORC Turbine for Laboratory Experiments, *Energy Proc.*, vol. 129, p. 1141-1148.

Søndergaard, R., Nielsen, O. J., Hurley, M. D., Wallington, T. J., & Singh, R., 2007, Atmospheric Chemistry of Trans-CF3CHCHF: Kinetics of the Gas-phase Reactions with Cl Atoms, OH Radicals, and O3, *Chem. Phy. Lett.*, vol. 443, p. 199-204.

Wheeler, A. P., & Ong, J., 2013, The Role of Dense Gas Dynamics on Organic Rankine Cycle Turbine Performance, *J. Eng. Gas Turbines Power*, vol. 135, no.10: p. 102603.

Wheeler, A. P., & Ong, J., 2014, A Study of the Three-dimensional Unsteady Real-gas Flows within a Transonic ORC Turbine, *ASME Turbo Expo 2014: Turbine Technical Conference and Exposition* (pp. V03BT26A003-V03BT26A003). American Society of Mechanical Engineers.

Woods, L. C., 1975, The Thermodynamics of Fluid Systems, *Oxford University Press*, ISBN 0 19 8561253.